MET.O.14

METEOROLOGICAL OFFICE
BOUNDARY LAYER RESEARCH BRANCH
TURBULENCE & DIFFUSION NOTE

T.D.N. No. 165

Observations of boundary layer structure made during the 1981 KONTUR experiment.

by A.L.M. Grant.

Dec. 1984.

Observations of boundary layer structure made during the 1981 KONTUR experiment

By A L M GRANT

Meteorological Office, Bracknell

1. Introduction

In some respects the boundary layer is one of the most important parts of the atmosphere since it is the region in which most of man's activities occur and through which the transfer of momentum, heat and moisture from the surface to the free atmosphere takes place. Except under very stable conditions (which can occur for example on clear, calm nights, or when air flows from the warm land over a cooler sea) the boundary layer is turbulent. A knowledge of the properties of atmospheric turbulence is important in structural design and in problems concerned with the dispersion of pollution in the atmosphere. The vertical transports of momentum, heat and moisture are important processes which have to be parametrized in numerical forecasting models.

The structure of the boundary layer over the sea will be described in this paper using data collected jointly by the Meteorological Office and the Max-Planck Institute for Meteorology in Hamburg. Mostly the data apply to a slightly unstable, inversion-capped boundary layer with non-precipitating clouds. Two different types of motion can be identified in the boundary layer studied here:

1) Three dimensional turbulence.
2) Two dimensional rolls.

Characteristics of both types of motion will be described.

2. Instruments, flight plans, intercomparisons and the data

The data to be described were collected by two aircraft during the KONTUR (Konvektion und Turbulenz) experiment over the German Bight. The two field phases of the experiment took place between 14 September and 21 October 1981. The aircraft, a Falcon 20 jet operated by the Deutsche Forschungs- und Versuchsanstalt fur Luft-und Raumfahrt and the Meteorological Research Flight C130, were capable of making high frequency measurements of temperature, humidity and the three wind components. The instruments used to collect the turbulence data are listed in Table I.

The flight patterns used in the experiment consisted of loosely co-ordinated 'L' patterns flown by the two aircraft in the subcloud and cloud layers. The legs of the 'L', which were between 40 km and 80 km long, were arranged to be parallel and perpendicular to the mean wind in the mixed layer. Before and after each experimental period the aircraft performed vertical soundings to determine the vertical structure of the lower atmosphere.

Analysis of data from several intercomparison runs, which were carried out during some of the flights, has shown that the agreement between the two aircraft for measurements of velocity and humidity fluctuations is generally good. This is further supported by the agreement between measurements obtained from the 'L' patterns and generally, no distinction is made in this paper between data collected by each of the aircraft. The agreement between heat fluxes in the intercomparisons was rather poor and they have been used here only to assess the stability of the boundary layer. Estimates of the Monin-Obukhov length, which is a measure of the relative importance of shear production of turbulence energy and buoyancy production, indicate that in most cases to be considered here buoyancy was not important in determining the structure of the turbulence.

Turbulence fluxes and variances were calculated for each run after the removal of any linear trends from the data using a least squares fit line. Surface fluxes were estimated by linear extrapolation of the data obtained at flight level to the surface. Spectra and cospectra were calculated using a fast fourier transform routine, after the removal of any linear trends from the data. For presentation, spectra are frequency weighted and plotted against log frequency (or wavenumber). Wind components (u, v, w) are with respect to a right-handed cartesian coordinate system with the x-axis along the mean boundary layer wind direction.

3. Weather conditions and the mean vertical structure of the lower atmosphere

Wind speeds in the mixed layer for the cases described were generally greater than 10 m/s, with wind directions ranging from southeast to west. Cumulus clouds were present on most occasions, though on 26 September the clouds cleared during the experiment. The clouds were sometimes aligned in streets approximately along the mean wind direction. Cloud streets are a common phenomenon in slightly unstable conditions with a reasonably large windspeed (Kuettner 1971), and are generally associated with a two-dimensional secondary flow in the boundary layer (Brown 1981). More will be said about these rolls below.

The vertical structure of the lower atmosphere is best illustrated using data from vertical soundings made during each experiment. Although these profiles are not as representative as those obtained from the horizontal 'L' patterns their vertical resolution is much greater so that regions of large vertical gradients are well resolved. Figure 1 shows profiles of virtual potential temperature (θ_v) and specific humidity (Q) obtained by the C130. Both variables show a well mixed layer extending from the surface in which vertical gradients are small. Above the mixed layer θ_v begins to increase with height and Q decrease. The cloud base was usually found close to the top of the mixed layer.

In a number of profiles, the v-component of the wind shows a layer of marked shear, starting near the top of the mixed layer, and extending through the inversion (Figure 2). Csanady (1974), using a simple model, has shown that the Ekman turning of the wind becomes concentrated in the inversion layer when the height of the lowest inversion is below the height to which turbulent mixing would extend in the absence of the inversion (i.e. 0.2 – 0.4 U_*/f; where U_* is the surface friction velocity and f is the Coriolis parameter). To see this, consider the u-component of the momentum equation;

$$f(V_g - V) = -\overline{du'w'}/dz \qquad -1$$

V_g= y-component of the geostrophic wind;

V = y-component of the mean wind;

$\overline{u'w'}$= x-component of the turbulent Reynolds stress.

where the local rate of change and advection terms have been neglected. It will be shown below that the turbulence stress profile is approximately linear in the mixed layer (i.e. $\overline{du'w'}/dz = U_*^2/Z_i$; where Z_i is the mixed layer depth), so:

$$(V - V_g)/U_* = U_*/(f\ Z_i) \qquad -2$$

Hence, within the mixed layer (V-Vg) is constant (and positive in the northern hemisphere), and the adjustment of the mixed layer wind to the geostrophic wind has to take place in the inversion layer. Estimates of $(V-V_g)/U_*$ and $U_*/(fZ_i)$ are shown in Table II, where (V-Vg) has been approximated by the observed shear. The agreement is quite good, although the variation in the estimates of (V-Vg) from different profiles on the same day can be large.

4. Similarity theory

Similarity theories provide a useful framework in which to analyse turbulence data and make comparisons with data collected in different conditions and over different surfaces. In these theories a small set of scaling parameters is assumed to describe the boundary layer. Dimensional analysis is used to obtain relationships between non-dimensional groups, constructed from the scaling parameters, and appropriately non-dimensionalised turbulence quantities.

Similarity theories describing the barotropic mixed layer use the same scaling parameters as the well known Monin-Obukhov surface layer similarity theory (e.g. Wyngaard 1973) plus the Coriolis parameter (f) and boundary layer depth (h). There are currently two choices for the boundary layer depth h:

a) $h \propto \frac{u_*}{f}$ (Blackadar and Tennekes 1968)

b) h=Zi=Height of the lowest inversion or the depth of the mixed layer (Deardorff 1972)

Deardorff (1972), using a large eddy model, found that even in slightly unstable conditions turbulent mixing extended up to the height of the inversion. Nicholls (1982) has found, experimentally, that this is not necessarily the case and that in slightly unstable conditions mixing may only extend up to $0.2U_*/f$. Table III shows that for some of the present data $fZi/U_* < 0.2$, i.e. vertical mixing is restricted by the inversion. In other cases the presence of cumulus clouds implies convective mixing up to cloudbase, the top of the mixed layer. In both cases the mixed layer depth is not determined by U_*/f and the appropriate form of the similarity hypothesis is:

$$X/X_* = F(Z/Zi, -Zi/L, U_*/fZi) \qquad -3$$

where:

X=Dimensional turbulence quantity

X*=Scaling parameter for X

Z=Height

L=Monin-Obukhov length

F=Empirically determined similarity function.

In the present data changes in the turbulence appear to be related to changes in stability and U*/fZi does not seem to be important in determining the properties of the boundary layer turbulence, although this may simply reflect the small range of values encountered.

Since the scaling parameters are based on surface fluxes the similarity hypothesis might not hold near the top of the boundary layer where entrainment may be important, and different scaling parameters appropriate (e.g. Guillemet et al (1983)).

5. Turbulence structure

a. Fluxes of momentum and moisture

Profiles of the x-component of the turbulent stress, normalised by the surface value and plotted against Z/Zi, are shown in Figure 3. The normalised stress decreases linearly from the surface value to zero at Z/Zi=1. At all levels in the boundary layer the transport of momentum is towards the surface.

Humidity flux profiles from three flights are shown in Figure 4. On 20 September and 29 September the humidity flux at the top of the mixed layer is similar to the surface flux. On 26 September the humidity flux decreases linearly with height so that the flux at the top of the mixed layer is only 10%-20% of the surface flux. The magnitude of the humidity flux at the top of the mixed layer, relative to that at the surface, appears to be related to the cloudiness. On both

20 September and 29 September cumulus clouds were present throughout the experimental period, while on 26 September the shallow cumulus clouds initially present cleared. LeMone and Pennell (1976) have also found small humidity fluxes at the top of the mixed layer in near cloud free conditions in the tropics. However, the results of a number of studies of the mixed layer humidity budget in the tropics show that, when averaged over a large area, the moisture flux at cloudbase is nearly equal to the surface flux. LeMone and Pennell argued that in order for their direct measurements to be consistent with the budget studies patches of small cumulus clouds must be very effective in removing water vapour from the mixed layer. Nicholls and LeMone (1980) reached similar conclusions about the importance of clouds to the mixed layer humidity budget in the tropics, using GATE aircraft data.

b. Velocity fluctuations

The non-dimensional velocity variance profiles in Figure 5 are similar to those obtained by Nicholls and Readings (1979) in the lower half of the boundary layer. Near surface values of σ_u^2/U_*^2 and σ_v^2/U_*^2 are in reasonable agreement with values obtained by Smith (1980) in neutral conditions and by Panofsky et al (1977) in more convective conditions. The near surface value for σ_w^2/U_*^2 is slightly smaller than found by Smith (1980). This could be due to a loss of high frequency variance at low levels in the aircraft data. A maximum in the σ_w^2/U_*^2 profile near the middle of the mixed layer, as seen on 29 September, has been reported by a number of workers (e.g. Caughey and Palmer 1979) in unstable conditions.

In the upper part of the mixed layer σ_u^2/U_*^2 and σ_v^2/U_*^2 are approximately equal and vary little with height, while σ_w^2/U_*^2 decreases slowly with height.

6. Spectral properties

In the surface layer one dimensional spectra of quantities which correlate with fluctuations in the vertical wind component have been found to differ significantly for sampling directions parallel and perpendicular to the mean wind direction (Nicholls and Readings 1981). Similar differences are observed here and spectra from the two sampling directions will be described separately.

a. Alongwind sampled spectra

The variation with height of the power spectra of the three wind components u,v,w is illustrated in Figure 6 using data from alongwind runs at heights between 30m and 300m carried out on 26 September. The spectra are characterised by a single peak, which in the case of u is rather broad and indistinct. In most of the mixed layer the positions of the peaks remain constant with height but near the surface ($Z/Zi<0.1$) those in the v and w spectra move to higher wavenumbers. The u spectrum does not appear to change shape near the surface. At high wavenumbers the spectra approach a -2/3 power law.

In order to compare the spectral shapes more easily it is useful to combine them using an appropriate normalisation. It is conventional to normalise spectra in such a way that they fall on a universal curve in the inertial subrange at large wavenumbers (e.g. Kaimal et al 1972) but since the present spectra are similar in shape throughout the mixed layer it is easier to normalise them by the total variance. The spectra obtained on 18, 26 (for $Z/Zi>0.2$) and 29 September (for $Z/Zi>0.05$), normalised in this way are shown in Figure 7. The wavenumber (K) has been non-dimensionalised using the mixed layer depth.

In near neutral conditions (represented by 18 September and 26 September) there is a broad peak in the u spectra between KZi=0.2 and 0.3 (wavelength between 3Zi and 5Zi). The u spectra obtained in more unstable conditions (29 September) are very similar to those obtained in neutral conditions. The peaks in the neutral v spectra occur at somewhat higher wavenumbers (around KZi=1.0) than the u spectral peaks. Under more unstable conditions the v spectra are flatter and a larger proportion of the total variance is contained at lower wavenumbers compared with the neutral spectra. Furthermore, in unstable conditions the u and v spectra are similar, as is found in convective conditions over land (Kaimal et al 1976).

Surface layer studies (e.g. Kaimal et al 1972) show that, in unstable conditions v spectra do not scale according to surface layer similarity. The surface layer v spectrum obtained on 29 September, the most unstable case considered, is similar to those obtained higher up in the mixed layer and has, in fact, been included in the normalised spectra shown in Figure 7. This similarity indicates that the fluctuations in v near the surface are influenced by large scale boundary layer motions, and explains the failure of surface layer scaling in unstable conditions. The acrosswind v spectrum in the surface layer is also similar to those in the rest of the mixed layer (see Figure 11). It might be expected, therefore, that in unstable conditions surface layer scaling should break down for acrosswind spectra as well.

b. Acrosswind sampled spectra

Figure 8 shows the acrosswind sampled spectra corresponding to those in Figure 6. As with the alongwind sampled spectra the acrosswind spectra all have a single peak which in the case of u and w tends to be narrower than the alongwind peak, particularly near the surface. The non-

dimensional wavelengths $\lambda_m(u)/Zi$ and $\lambda_m(w)/Zi$, of the peaks in the u and w spectra are shown in Figures 9 and 10, plotted against Z/Zi. Both increase approximately linearly with height up to Z/Zi=0.2-0.3 and are constant over the rest of the mixed layer, although there appears to be an increase in $\lambda_m(u)/Zi$ near the top of the layer which could be due to either entrainment or variations in the depth of the mixed layer.

The variation of $\lambda_m(w)/Zi$ with height is similar to that found for alongwind spectra in the convective mixed layer overland (Kaimal et al 1976) and for acrosswind spectra in the convective mixed layer over the sea (Nicholls and LeMone 1980). In the JASIN experiment the mixed layer was not capped by an inversion (i.e. $h \propto \frac{u_*}{f}$) and Nicholls (1982) found that $\lambda_m(w)/h$ increased linearly with height throughout the mixed layer. It is likely that the difference between the KONTUR and JASIN results is due to the effect of the inversion, and not stability, on the turbulence structure, since in neither case were conditions particularly unstable. In the mixed layer $\lambda_m(w)/Zi$ varies between 0.8 and 1.5. Some of this variation might be due to stability since the smallest values of $\lambda_m(w)/Zi$ were found on 18 and 26 September, both occasions of near neutral stability. Such a variation would be in line with surface layer data (Kaimal et al 1982). The larger values of $\lambda_m(w)/Zi$ are similar to those reported by Kaimal et al (1976) and Nicholls and LeMone (1980), both of whom found $\lambda_m(w)/Zi$ to be approximately 1.5 in the convective mixed layer.

The difference between the u spectra in the alongwind and acrosswind directions near the surface has been mentioned above (cf Figures 6 and 8). While the position of the peaks in the acrosswind spectra scale with Z, the alongwind u spectrum at $Z \approx 0.1Zi$ is very similar to those higher in the mixed layer i.e. it appears to scale with Zi. Kaimal et al

(1982) also found that u spectra, collected from the Boulder Atmospheric Observatory tower in windy conditions, do not vary much with height above 0.1Zi. In the surface layer Nicholls and Readings (1981) attribute the differences that they observed between spectra from the two sampling directions to the stretching of eddies by the mean shear. Figures 9 and 10 suggest that the presence of an inversion limits the size of eddies to a few times the depth of the mixed layer, and because of the stretching of the eddies in the surface layer the effects of the inversion are apparent in the alongwind spectra at a lower height than in the acrosswind spectra. The effect of shear on the momentum-carrying eddies is similar to that on the 'u' eddies, which is not surprising since eddies with a good correlation between u and w should interact strongly with the mean shear to produce turbulent energy (Tennekes and Lumley 1972). Like the u spectra, the uw cospectra have a single main peak. In the acrosswind direction the wavelength of the peak varies with height in the same way as $\lambda_m(u)$ (Figure 9) but in the alongwind direction the wavelength of the peak (approximately 2Zi) is constant with height at the levels accessible to the aircraft ($Z>0.1Zi$).

The behaviour of the acrosswind sampled v spectra is complicated by the presence of horizontal roll vortices in the mixed layer, as shown in Figure 11 for 18 September. Near the surface ($Z<0.35Zi$) the spectra have a peak around $KZi=1.0$ and are similar to the alongwind spectra. This agrees with the findings of Nicholls and Readings (1981) in the surface layer. Above $Z=0.35Zi$ the peak moves to slightly smaller wavenumbers around $KZi=0.5$, a scale characteristic of horizontal roll vortices.

In more unstable conditions (29 September) most of the v energy is concentrated around $KZi=0.4$ in contrast to the rather flat alongwind spectra. Again roll vortices probably

provide the reason for this difference (although the cloud cover was rather random on this day). The existence of rolls in this case is consistent with the findings of LeMone (1973) who reported rolls for $-Zi/L<10$ compared to the present value of 6 (see Table III). The w spectral peak at $\lambda=1.5Zi$ (see Figure 10) in the mixed layer, which is characteristic of thermals (Kaimal et al 1976) shows that the roll motion probably coexists with a considerable amount of three dimensional convection, as has been observed for instance by Konrad (1970) using a clear air doppler radar.

7. Two dimensional roll motions in the boundary layer

The preceding sections have concentrated on the characteristics of the turbulent fluctuations and the net transport of momentum and moisture in the subcloud layer. Since Woodcock's (1941) observations of the soaring behaviour of seagulls revealed the existence of 'linear convection' there has been a considerable effort to study roll vortices in the boundary layer (e.g. Brown 1970, LeMone 1973).

On 20 September small cumulus clouds at the top of the mixed layer were aligned into streets, suggesting that horizontal roll vortices were present in the boundary layer. Indeed roll motions encountered on the alongwind runs distorted the velocity spectra which were therefore not shown in Figure 7. The acrosswind v spectra have a peak around $\lambda=3Zi$ (Figure 12). The separation of the cloud lines, determined using a radiometer, varied between 2 km and 3.7 km with an average separation of 2.6 km (3.4Zi), in good agreement with the position of the v spectral peak. The wavelength of the peak and the separation between the cloud lines are in good agreement with previous determinations of the scale of roll vortices and with theoretical analyses (LeMone 1973).

The clouds provide a reference which allows a picture of any roll circulation in the mixed layer, which might be associated with the cloud lines, to be obtained by averaging data from several rolls together, in much the same way as LeMone (1976). The results are shown in Figure 13. The flow is divergent between the cloud lines near the surface and convergent higher up, consistent with a two dimensional roll circulation in a plane perpendicular, or nearly perpendicular, to the mean wind. The air between cloud lines is relatively drier than the air beneath the lines. This difference can be traced to near the surface. LeMone and Pennell (1976) have observed a similar sort of eddy structure in the mixed layer, which was associated with streets of small cumulus.

The correlation between the vertical velocity and humidity field in Figure 13 implies that the roll motion transports moisture. Cospectra of humidity and vertical velocity in Figure 14 show that in the upper part of the boundary layer an appreciable fraction of the water vapour flux is in fact carried at scales comparable to the separation of the cloud lines. At $Z/Zi=0.7$ the flux carried by the rolls (estimated from Figure 13) is approximately 40% of the total flux. Nearer the surface the transport of water vapour is accomplished by smaller scale turbulence.

8. Summary

Data collected throughout the depth of the boundary layer, in conditions ranging from nearly neutral to unstable, have been presented. The characteristics of three dimensional turbulent fluctuations have been described and the effect of the low level inversion on turbulence length scales illustrated. In addition to the three dimensional turbulence field, two dimensional roll vortices were also present in the mixed layer on a number of days. One particularly clear case was used to illustrate the roll

circulation in the mixed layer and estimate the amount of moisture transported by the rolls. In the upper part of the boundary layer the transport of moisture by the roll circulation was significant.

Spectra from the most unstable day considered here (for which $-Zi/L=6$) suggest that roll convection and more random three dimensional convection co-existed in the mixed layer, although the cloud patterns were not strongly influenced by the presence of rolls.

Table I. Instruments used on the Falcon 20 and the C130 to collect turbulence data.

Meteorological variable.	Falcon 20 Instrumentation.	C130 Instrumentation.
Wind components. (u,v,w)	Pitot static probe. Flow angle sensor. Inertial navigation system.	Pitot static probe. Angle of sideslip vane. Angle of attack vane. Inertial navigation system.
Temperature(T).	Rosemount, reverse flow, open wire, platinum resistance thermometer. Pitot static probe.	Rosemount, reverse flow, open wire, platinum resistance thermometer. Pitot static probe.
Specific Humidity(Q).	Vaisala Humicap. Lyman α Humidiometer.	Dewpoint hygrometer. Microwave refractometer.

Table II. Average values of $\frac{(V-Vg)}{U_*}$. The uncertainties quoted for $\frac{(V-Vg)}{U_*}$ represent the variability in $(V-Vg)$.

Date/Flight number.	$(V-Vg)$ m s^{-1}	$\frac{(V-Vg)}{U_*}$	$\frac{U_*}{f\ Zi}$
18 September. H460	8.5	14.9 ± 2.4	13.6
22 September. H462	3.8	15.5 ± 8.9	17.0
26 September. H465	6.0	12.1 ± 6.3	9.8
Average value of $\frac{(V-Vg)\ f\ Zi}{U_*^2}$ = 1.06 ± 0.14			

Table III. Estimates of parameters relevant to boundary structure.

Date/Flight number.	Z_i (m)	cloud base (m)	$\frac{Z_i}{L}$	$\frac{f\ Z_i}{U_*}$	Comments.
18 September. H460	350	270-330	0.6	0.07	Cloud streets reported.
20 September. H461	770	760-850	1.0	0.15	Cloud streets reported.
22 September. H462	120	-		0.06	No clouds reported. Shallow mixed layer.
26 September. H465	430	500	0.8	0.10	Cloud streets reported at start of experiment. Cloud had cleared by the end of the period.
29 September. H467	700	800-830	5.9	0.28	Non-precipitating cumulus clouds at the top of the mixed layer.
10 October. H471	1000	1000	1.6		Frequent heavy showers reported.

References.

Blackadar,A.K., and Tennekes,H., 1968: Asymtotic similarity in neutral barotropic atmospheric boundary layers. J. Atmos. Sci.,25,1015-1020.

Brown,R.A., 1970: A secondary flow model for the planetary boundary layer. J. Atmos. Sci.,27, 742-757.

Caughey,S.J. and Palmer,S.G., 1979: Some aspects of turbulence structure through the depth of the convective boundary layer. Quart. J. R. Met. Soc., 105,811-827.

Csanady,G.T., 1974: Equilibrium theory of the planetary boundary layer with an inversion lid. Boundary-layer Meteor.,6,63-79.

Deardorff,J.W., 1972: Numerical investigation of neutral and unstable planetary boundary layers. J. Atmos. Sci.,29,91-115.

Guillemet,B.,Isaka,H. and Mascart,P., 1983: Molecular dissapation of turbulent fluctuations in the convective mixed layer·Part 1:Height variations of the dissapation rates. Boundary-layer Meteor.,27,141-162.

Kaimal,J.C., Wyngaard,J.C., Izumi,Y., and Cote, O.R., 1972: Spectral characteristics of surface layer turbulence. Quart. J. R. Met. Soc.,98, 563-589.

Kaimal,J.C., Wyngaard,J.C., Haugen,D.A., Cote,O.R., Izumi,Y., Caughey,S.J., and Readings, C.J., 1976: Turbulence structure in the convective boundary layer. J. Atmos. Sci.,33, 2152-2169.

Kaimal,J.C., Eversole,R.A., Lenschow,D.H., Stankhov,B.B., Kahn,P.H. and Businger,J.A., 1982: Spectral characteristics of the convective boundary layer over uneven terrain. J. Atmos. Sci., 39,1098-1114.

Konrad,T.G., 1970: The dynamics of the convective process in clear air as seen by radar. J. Atmos. Sci.,27,1138-1147.

Kuettner,J., 1971: Cloud bands in the earths atmosphere:Observations and theory. Tellus,23,404-425.

List of Figures.

Figure 1. Vertical profiles of virtual potential temperature (Θ_v) and specific humidity(Q) obtained by the C130.Each point is an average over a vertical distance of 10m to 25m,depending on the rate of ascent or descent.The short horizontal lines mark the positions of cloud base and cloud top,estimated by the aircraft scientist.Details of the flights can be found in Table III.

Figure 2. Vertical profiles of the y-component of the wind, obtained by the C130,showing the vertical shear in the inversion layer.Each point is an average over a vertical distance of 10m to 25m,depending on the rate of ascent or descent.The short horizontal lines mark the top and bottom of the inversion layer.Estimates of (V-Vg) are given in Table II.

Figure 3. Profiles of the non-dimensional x-component of the turbulent stress.Each point represents an average over one leg of an 'L'.Data from both aircraft are included but no distinction is made between them.The closed symbols are for near neutral conditions and the open symbols for more unstable conditions.

Figure 4. Vertical humidity flux profiles for three flights. All the height scales have been normalised to the mixed layer depth Z_i for convenience but the flux values are dimensional.The fluxes obtained by the Falcon 20 are denoted by the ringed symbols,while those from the C130 are denoted by the plain symbols.On 20 September only those fluxes obtained on acrosswind runs are plotted(for reasons given in section 7).

Figure 5. Vertical profiles of the non-dimensional wind component variances: a) longitudinal wind component (u); b) lateral wind component (v); c) vertical wind component (w). The arrows on the horizontal axes show the surface layer values obtained by Smith(1980) (S) and Panofsky et al (1977) (P).The curves represent the results of Nicholls and Readings (1979).For details of symbols etc.see Figure 3.

Figure 6. Power spectra of the three wind components (u,v and w) obtained on alongwind runs on 26 September for heights between 30m and 300m.In this and subsequent figures showing spectral data,the ordinate is the frequency weighted power spectrum.

Figure 7. Normalised power spectra of the horizontal wind components u and v obtained on alongwind runs on 18,26 and 29 September.The spectral estimates have been normalised by the total variance and the wavenumber by the mixed layer depth.The data for 18 and 26 September are for near neutral conditions and the data for 29 September are for more unstable conditions.

Figure 8. The same as for Figure 6 but for acrosswind runs.

Figure 9. Variation of the wavelength of the peak in the acrosswind u spectrum(numbers) and the uw cospectrum(circles) with height.The mixed layer depth has been used to normalise both the wavelength of the peak and the height.The curve represents the line $\lambda_m(u)=7Z$.

Figure 10. The same as for Figure 9 but for the w spectral peak only.The curves represent $\lambda_m(w)=3.3Z$ and $\lambda_m(w)=5Z$.

Figure 11. Normalised v spectra obtained on acrosswind runs on 18 and 29 September.The normalisation is the same as in Figure 7.

Figure 12. v spectra obtained on acrosswind runs,below cloud base,on 20 September.The small arrows indicate the range of separations between cloud lines,determined from radiometer data.(note,to convert frequencies into wavenumbers, divide by 100).

Figure 13. Cross section in the yz plane of the perturbations in the velocity components v and w,and the specific humidity, which are related to cloud lines.At each level data from several pairs of cloud lines have been averaged ,after the removal of the local means,to produce a composite.

Figure 14. Humidity flux cospectra obtained on acrosswind runs on 20 September.As in Figure 12 the small arrows on the frequency scale indicate the cloud line separations determined from radiometer data.

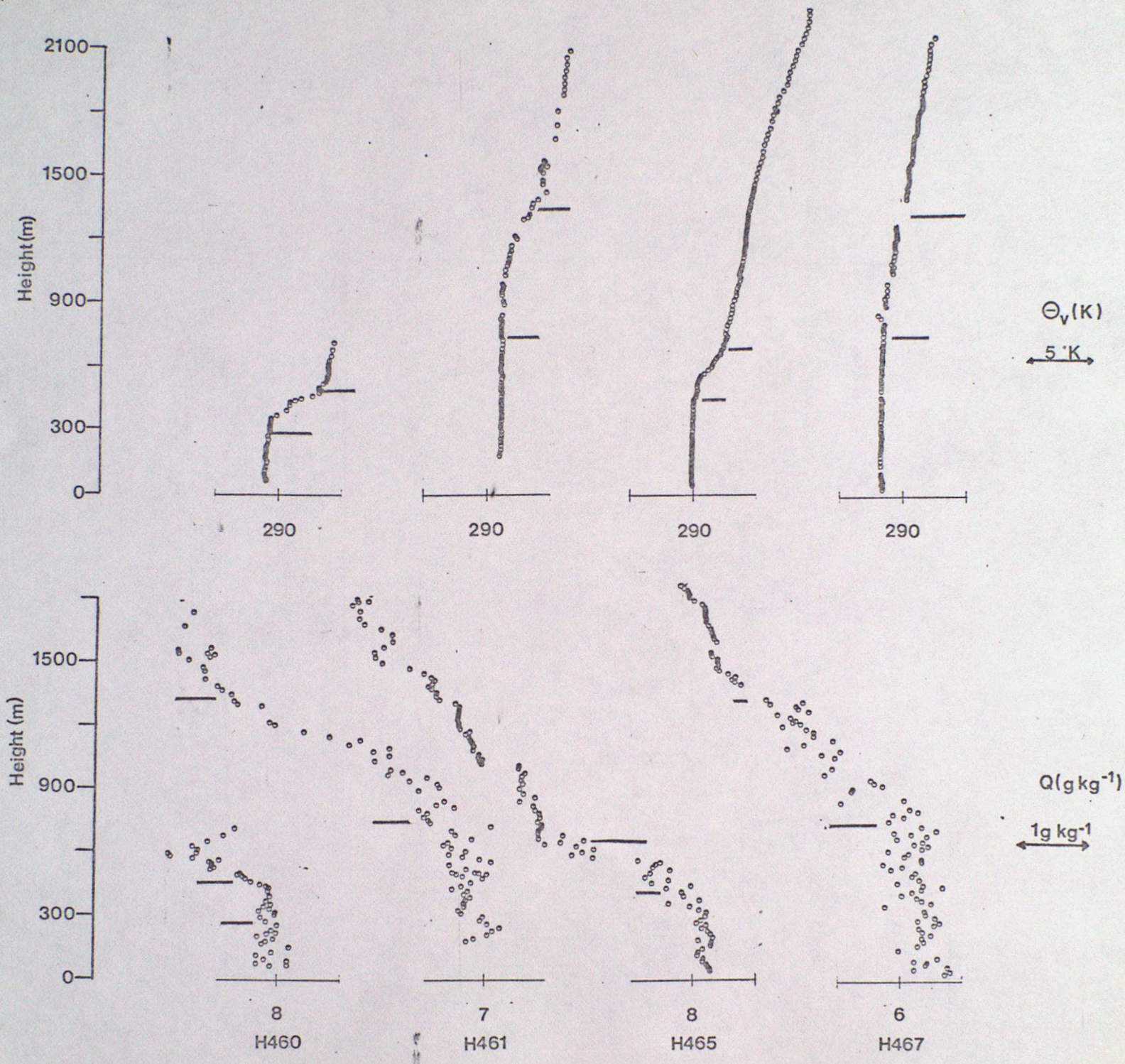
2100
1500
900
300
0
Height(m)
290
290
290
290
Θ_v(K)
5 K
1500
900
300
0
Height (m)
8
H460
7
H461
8
H465
6
H467
Q(g kg^{-1})
1g kg^{-1}

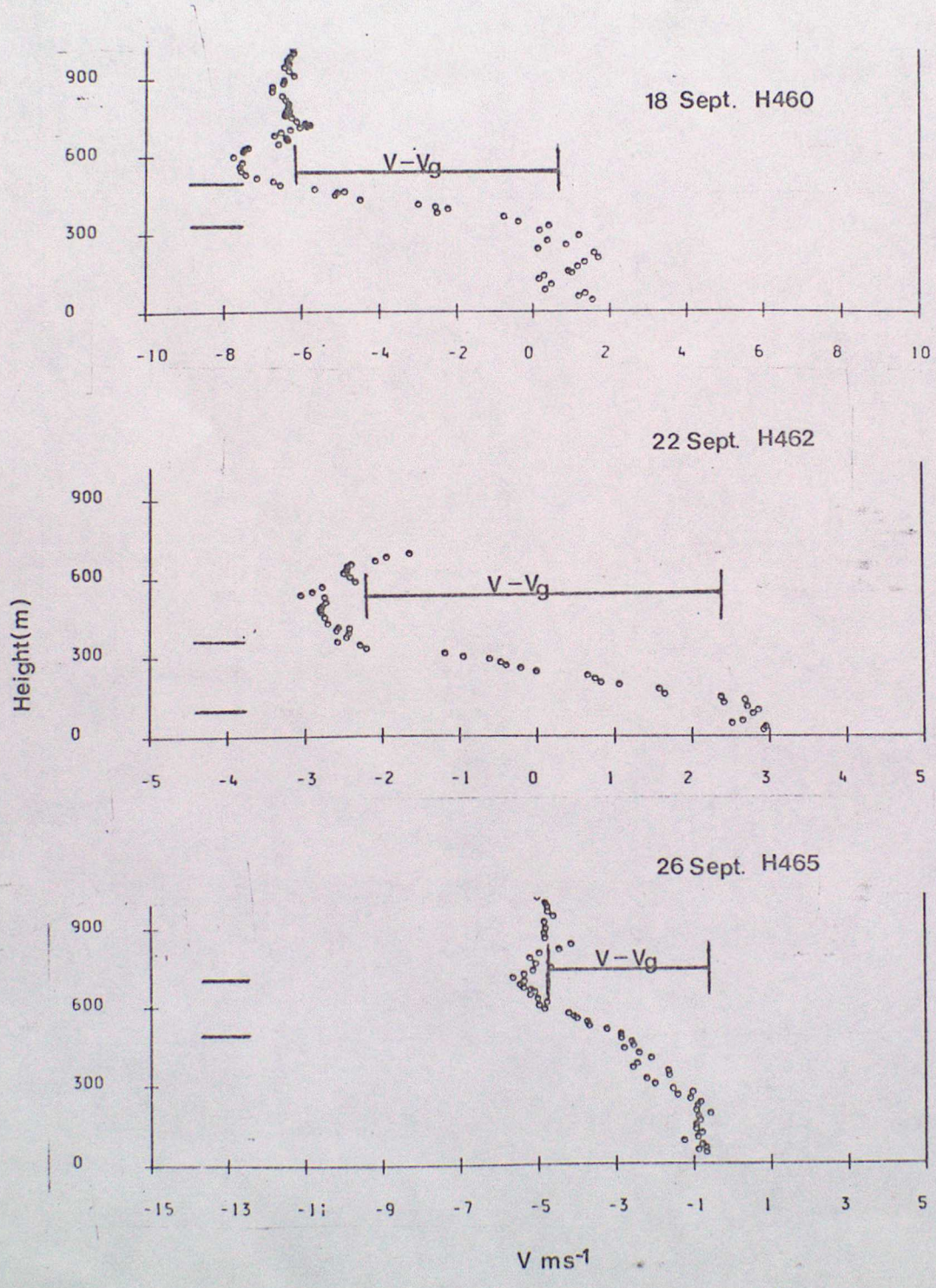
18 Sept. H460
V−Vg
900
600
300
0
-10
-8
-6
-4
-2
0
2
4
6
8
10
22 Sept. H462
V−Vg
900
600
300
0
-5
-4
-3
-2
-1
0
1
2
3
4
5
Height(m)
26 Sept. H465
V−Vg
900
600
300
0
-15
-13
-11
-9
-7
-5
-3
-1
1
3
5
V ms-1

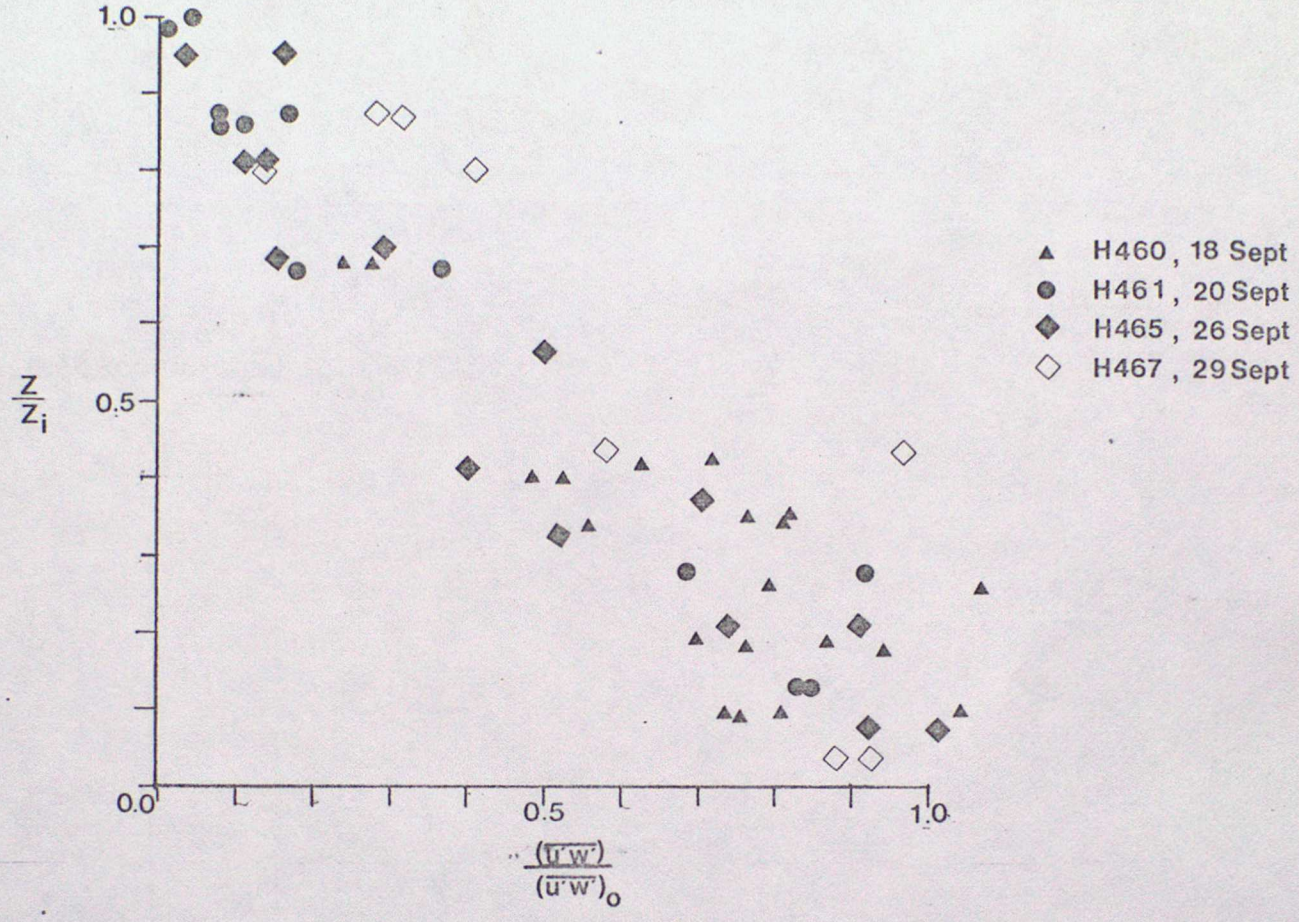
1.0
0.5
0.0
0.5
1.0
$\frac{z}{z_i}$
$\frac{(\overline{u'w'})}{(\overline{u'w'})_o}$
H460, 18 Sept
H461, 20 Sept
H465, 26 Sept
H467, 29 Sept

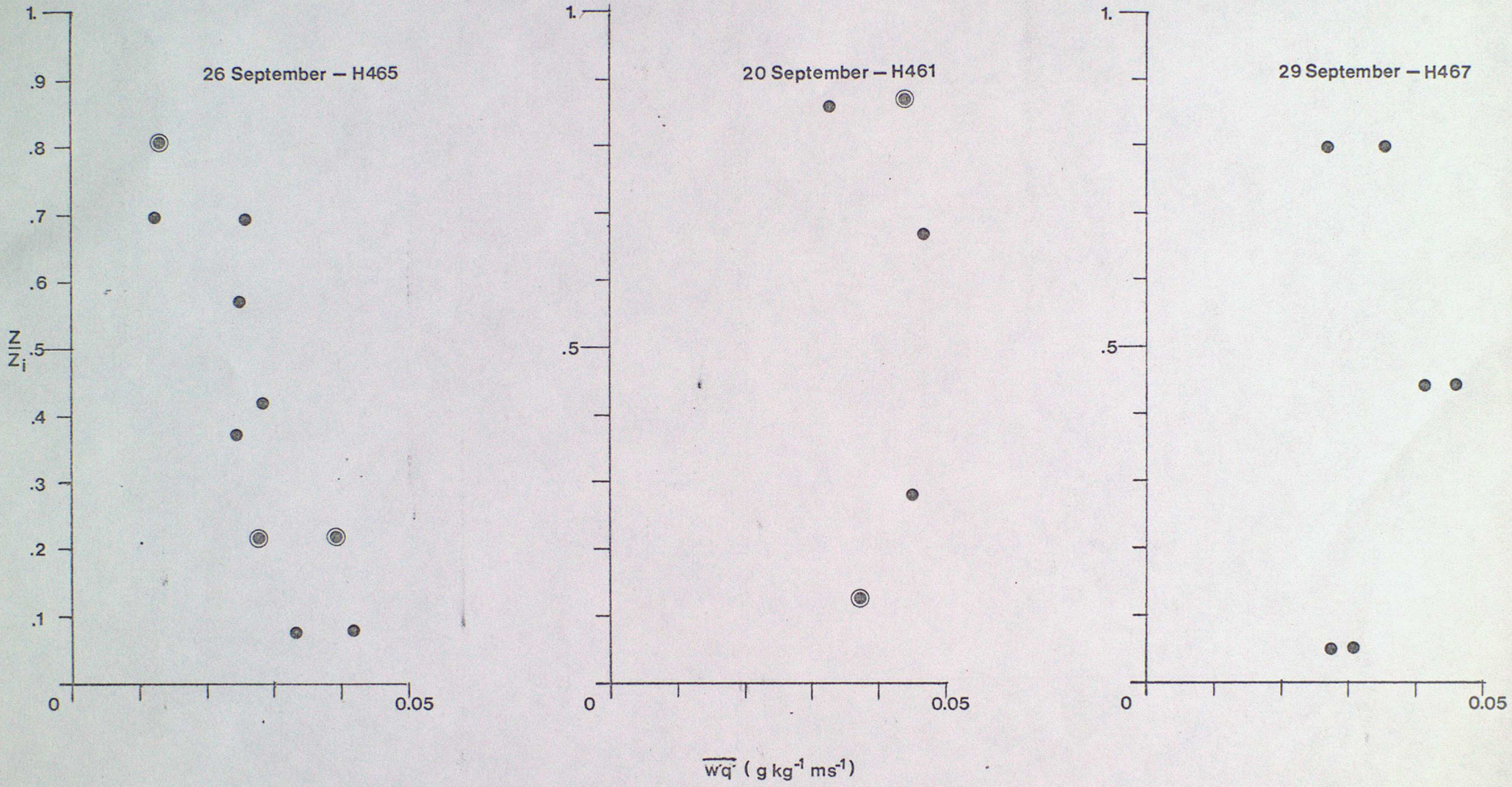
26 September — H465
20 September — H461
29 September — H467
1.
.9
.8
.7
.6
.5
.4
.3
.2
.1
0
0.05
Z/Zi
w'q' (g kg-1 ms-1)

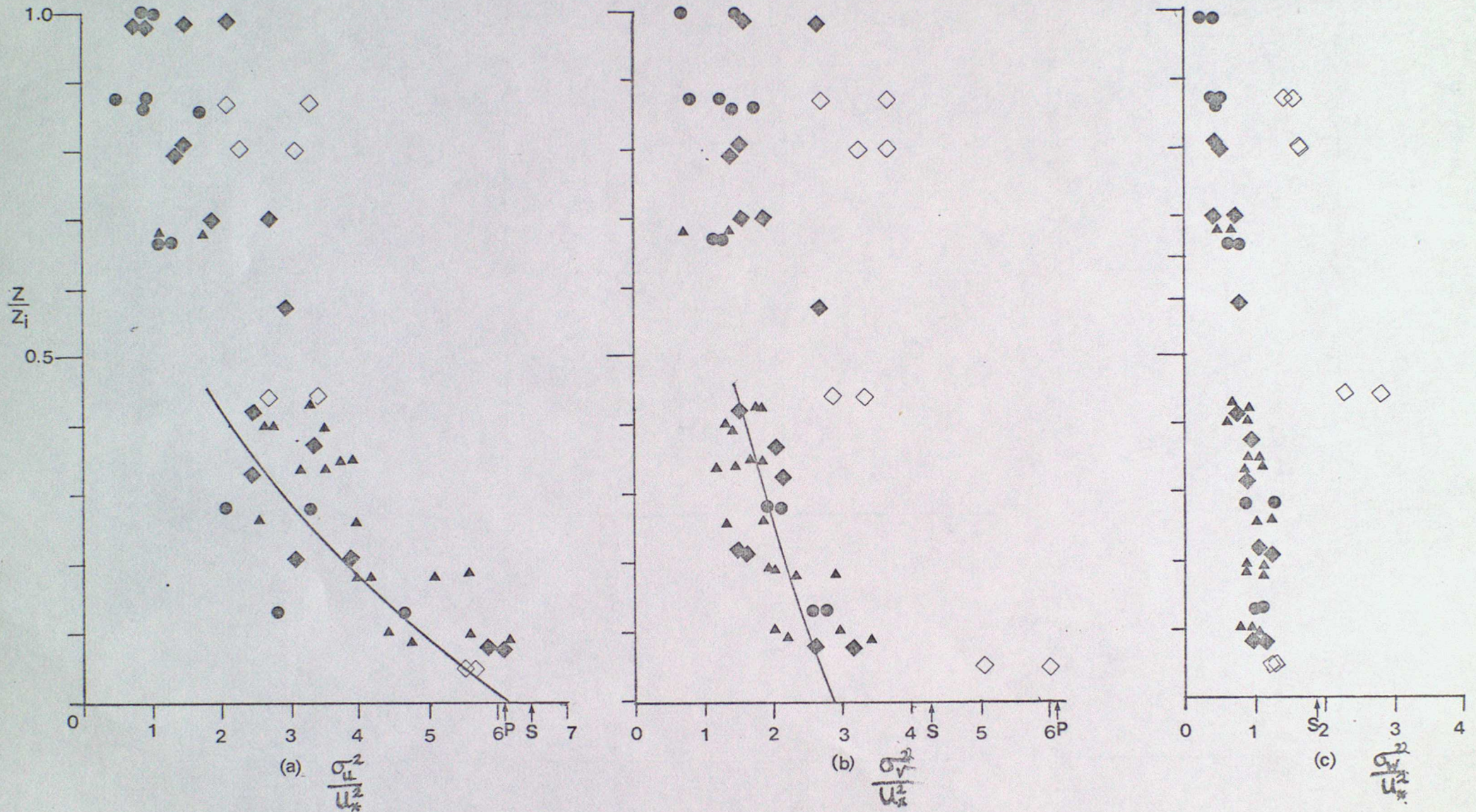
1.0
0.5
0
$\frac{z}{z_i}$
1
2
3
4
5
6
P
S
7
(a) $\frac{\sigma_u^2}{u_*^2}$
0
1
2
3
4
S
5
6
P
(b) $\frac{\sigma_v^2}{u_*^2}$
0
1
S2
3
4
(c) $\frac{\sigma_w^2}{u_*^2}$

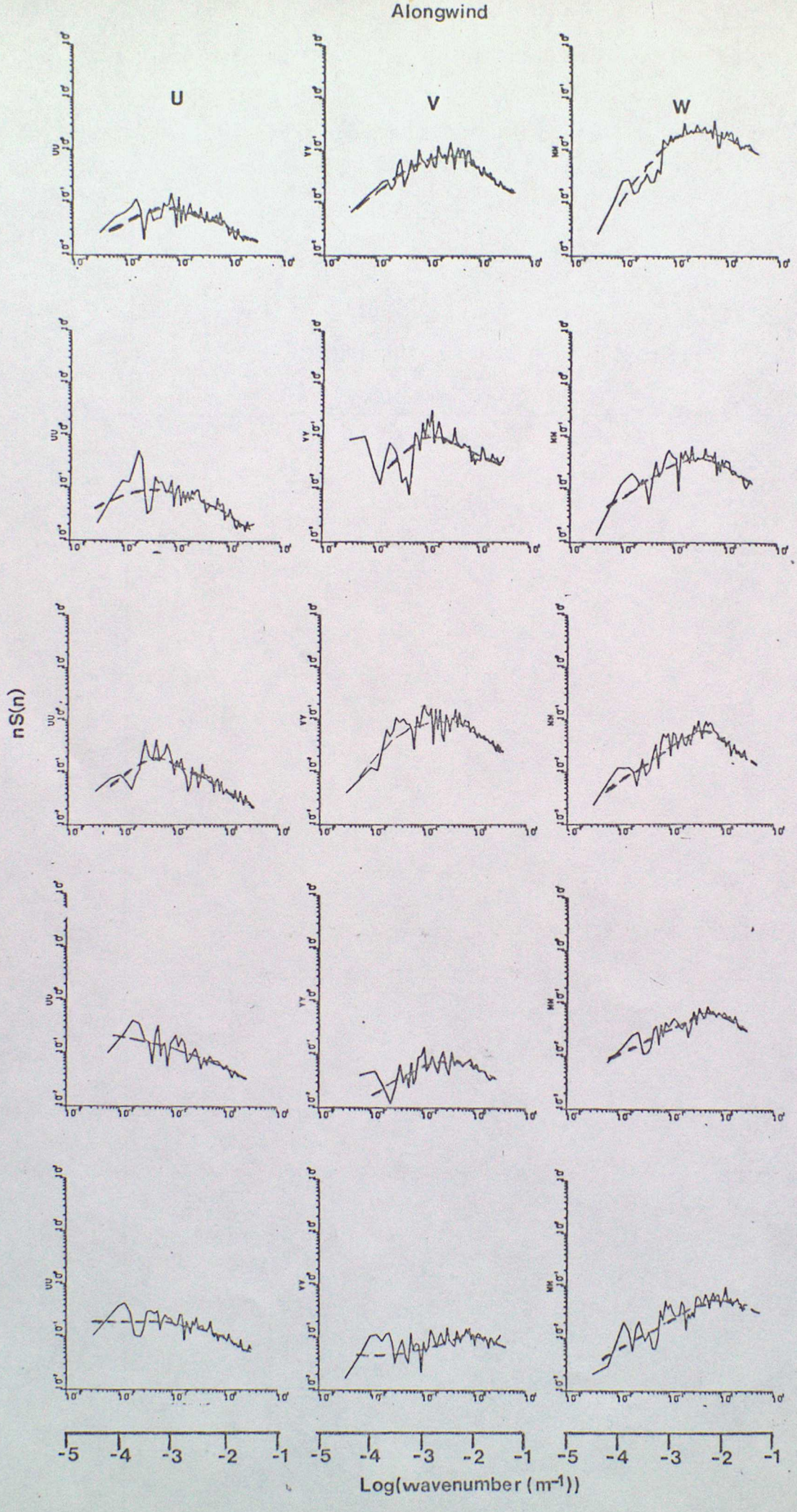
Alongwind
U
V
W
z/zi
0.69
0.58
0.37
0.21
0.08
nS(n)
-5 -4 -3 -2 -1
Log(wavenumber (m⁻¹))

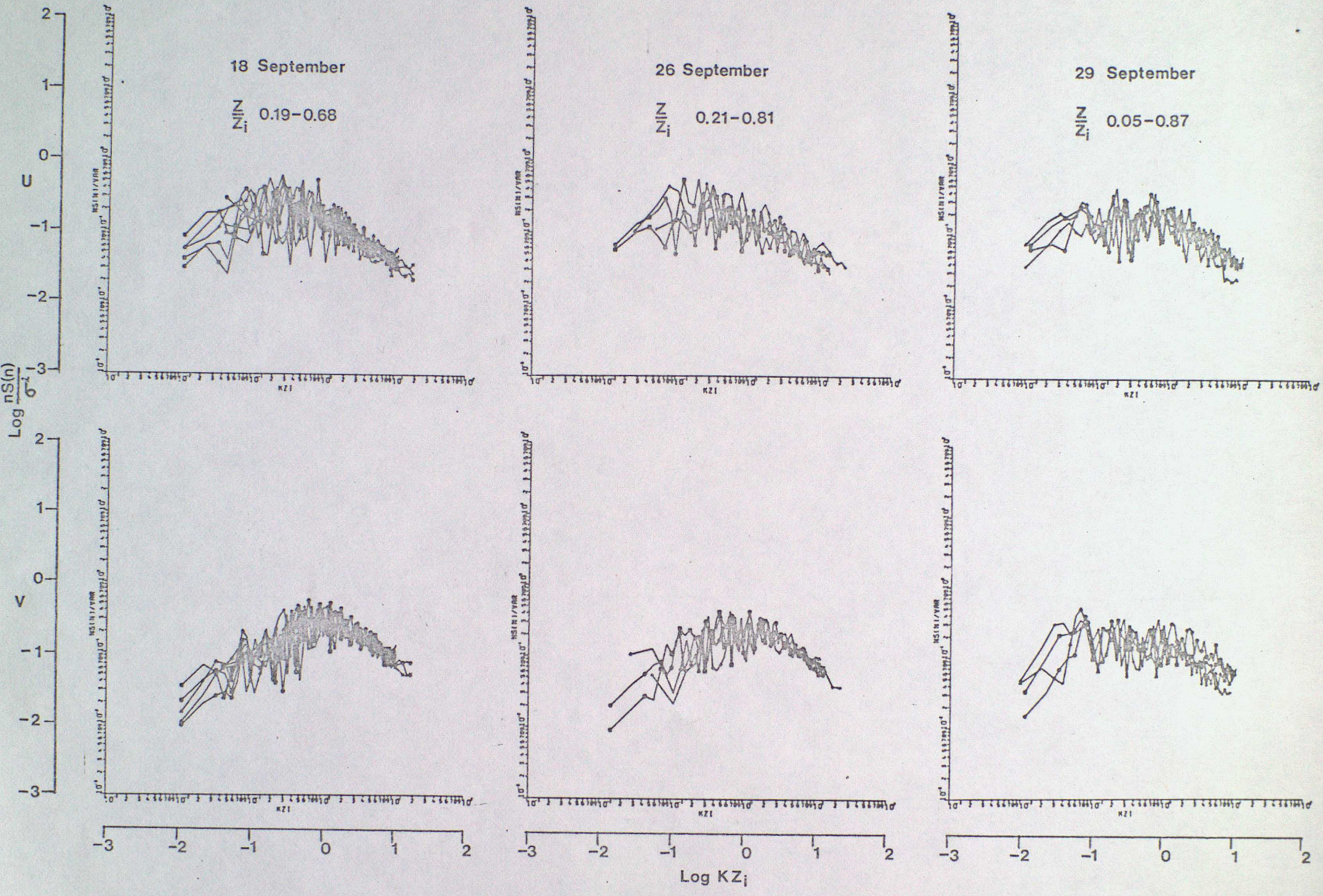
18 September
Z/Zi 0.19–0.68
26 September
Z/Zi 0.21–0.81
29 September
Z/Zi 0.05–0.87
U
V
Log nS(n)/σ²
Log KZi
KZI
2
1
0
−1
−2
−3

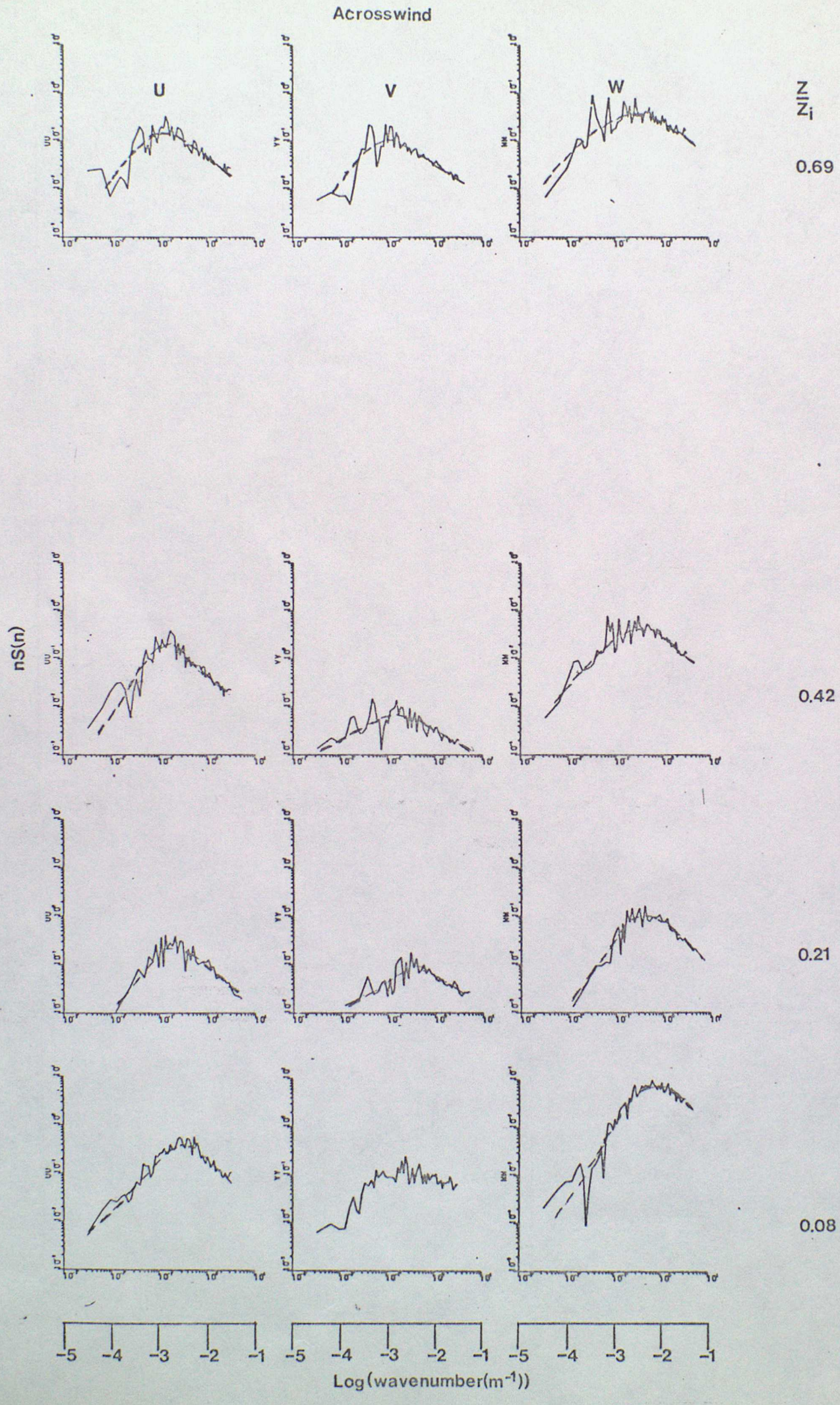
Acrosswind
U
V
W
Z/Zi
0.69
0.42
0.21
0.08
nS(n)
-5 -4 -3 -2 -1
Log(wavenumber(m-1))

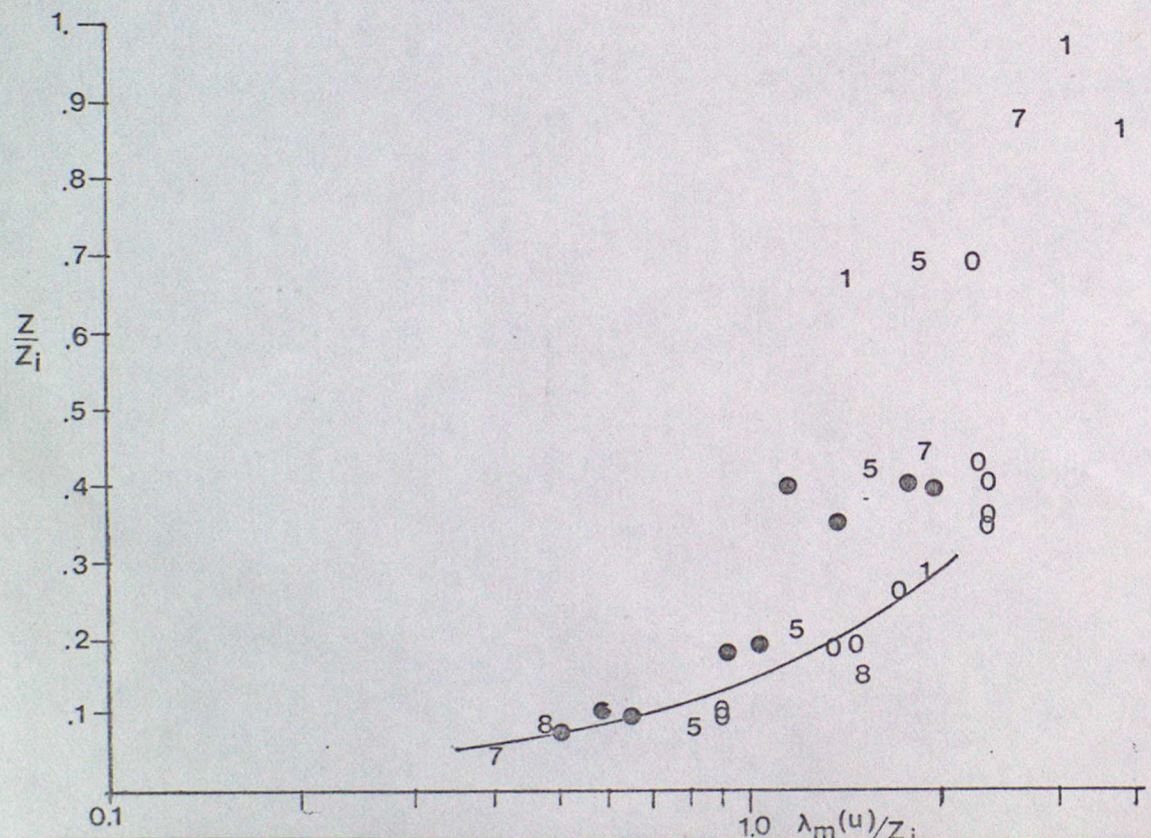
1.
.9
.8
.7
.6
.5
.4
.3
.2
.1
Z/Zi
0.1
1.0
λm(u)/Zi
0 H460, 18 Sept
1 H461, 20 Sept
5 H465, 26 Sept
7 H467, 29 Sept
8 H471, 10 Oct
λm(u)/Zi
λm(uw)/Zi

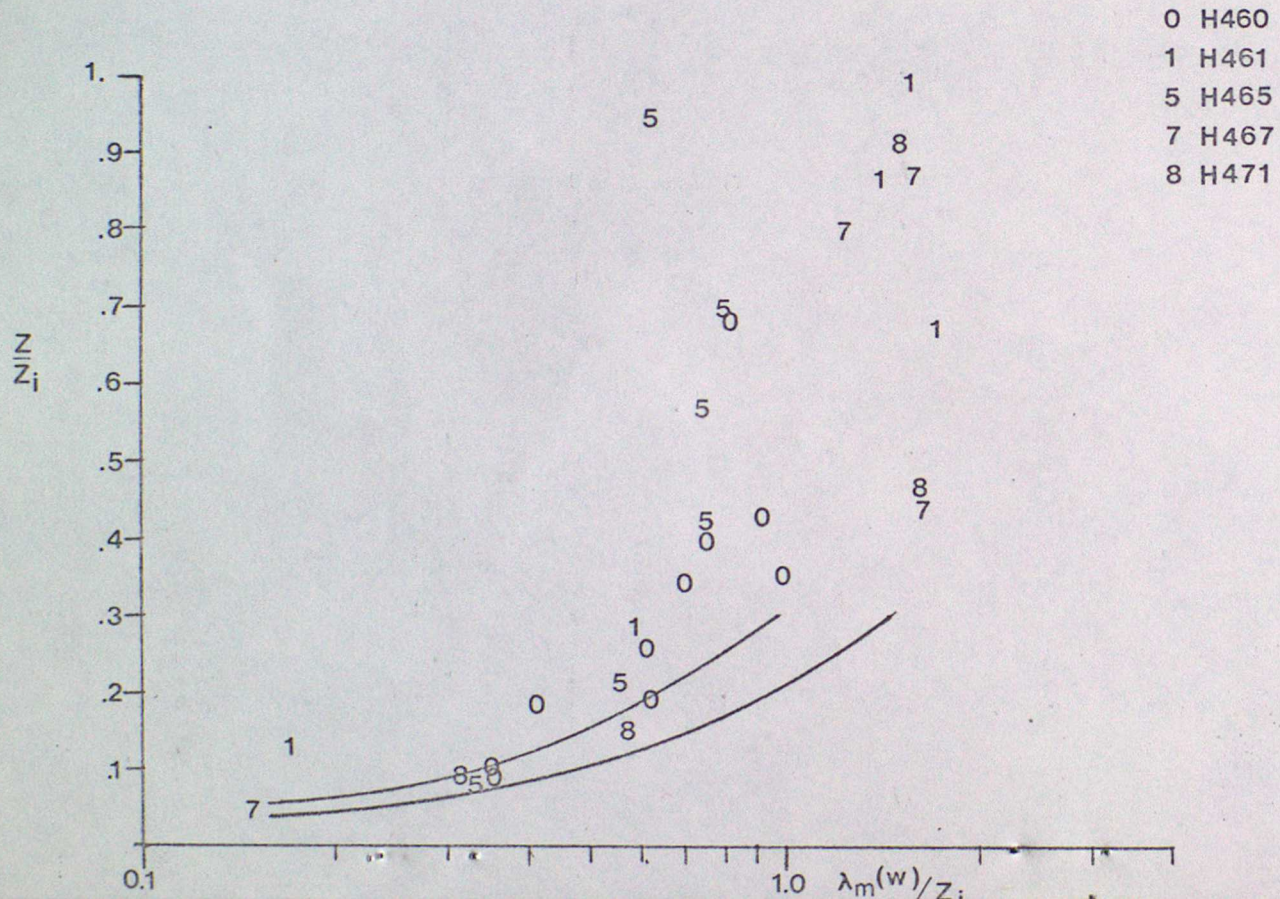
0 H460
1 H461
5 H465
7 H467
8 H471
1.
.9
.8
.7
.6
.5
.4
.3
.2
.1
Z/Zi
0.1
1.0
λm(w)/Zi

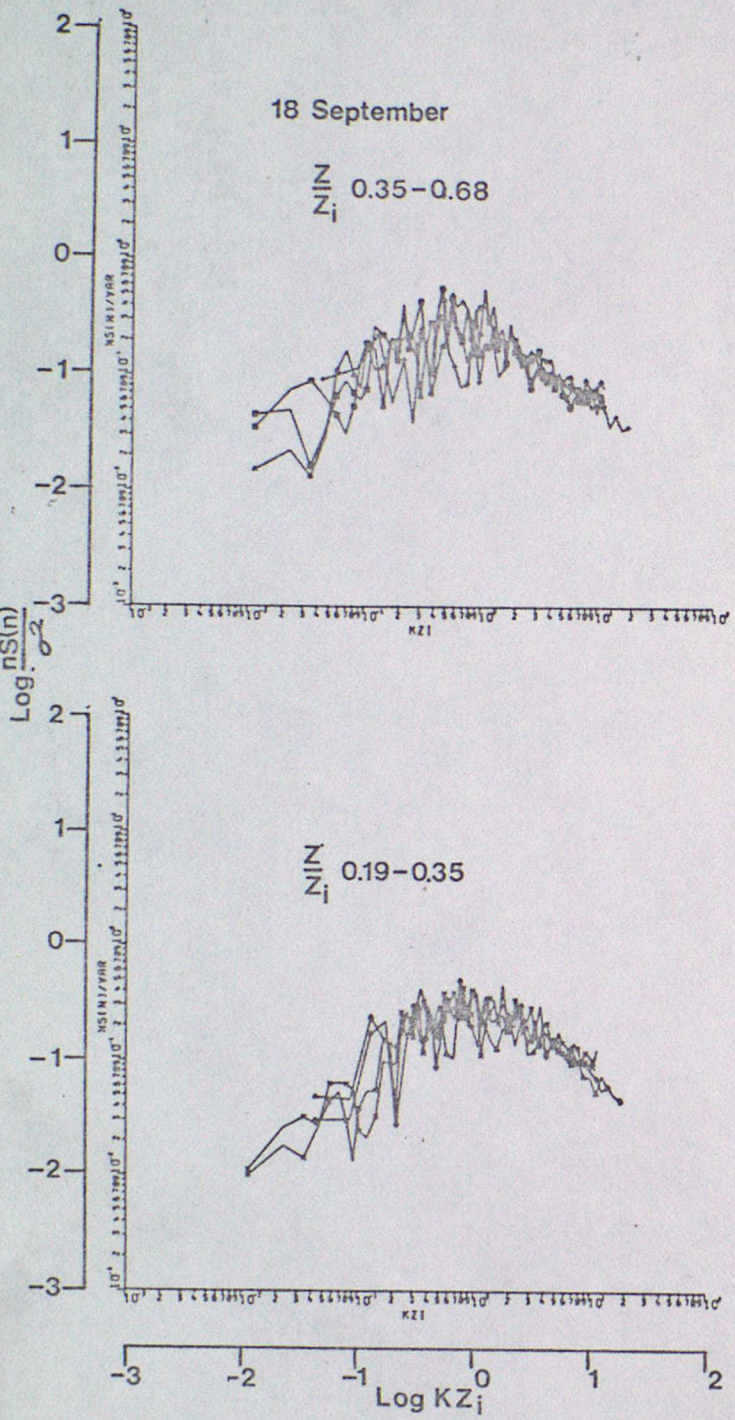
18 September
$\frac{Z}{Z_i}$ 0.35–0.68
$\frac{Z}{Z_i}$ 0.19–0.35
$\text{Log}\frac{nS(n)}{\sigma^2}$
2
1
0
−1
−2
−3
KZI
−3
−2
−1
0
1
2
Log KZ_i

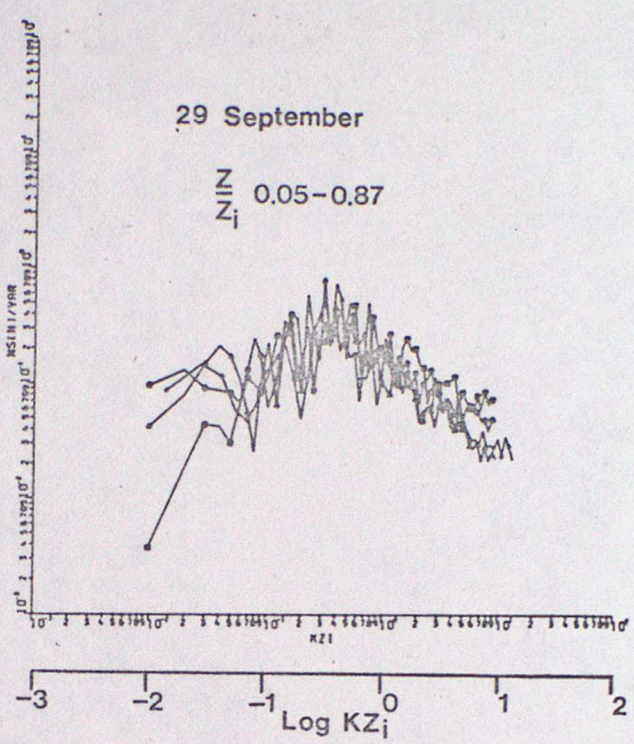
29 September
$\frac{Z}{Z_i}$ 0.05–0.87
KZI
−3
−2
−1
0
1
2
Log KZ_i

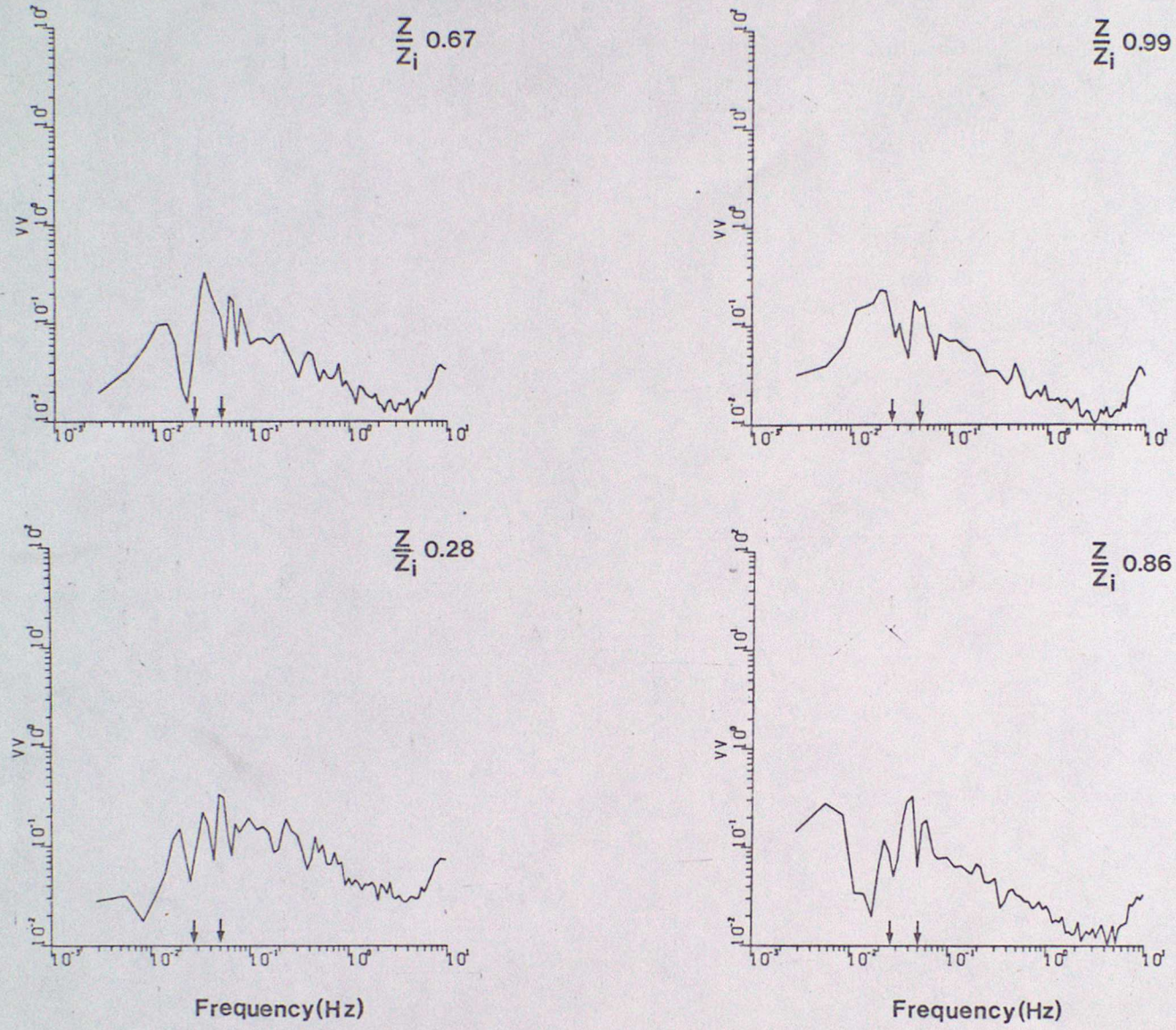

20 September 1981 (Z_i 770m)

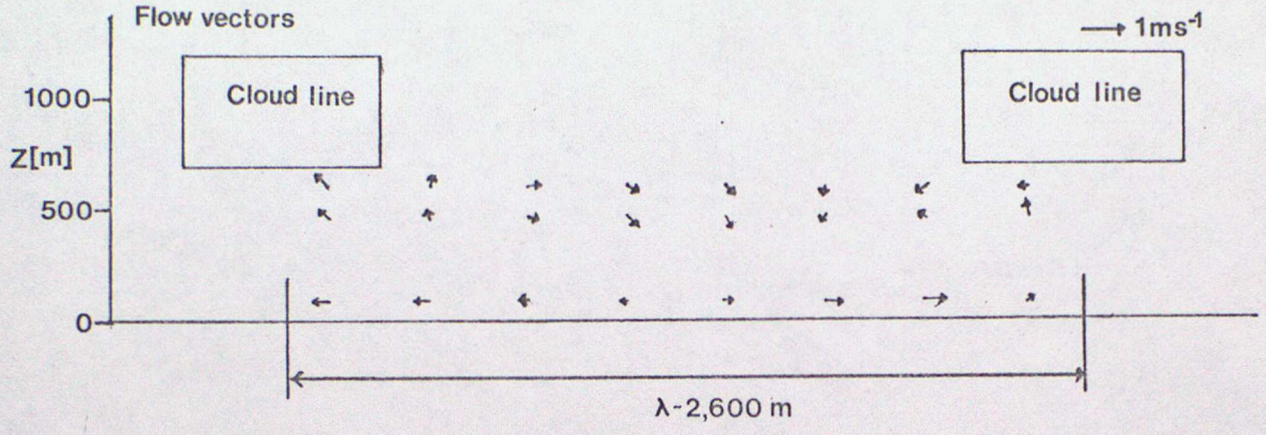
Flow vectors
1ms-1
Cloud line
Cloud line
1000
Z[m]
500
0
λ-2,600 m

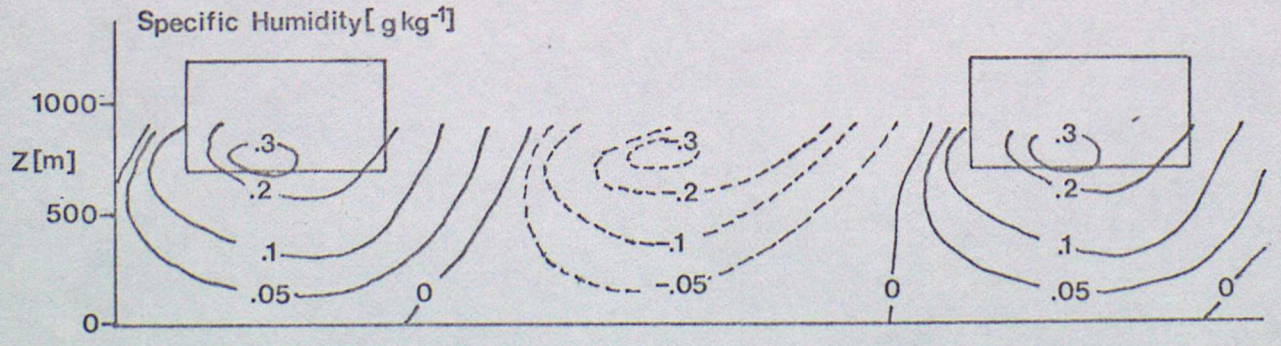
Specific Humidity[g kg-1]
1000
Z[m]
500
0
.3
.2
.1
.05
0
-.3
-.2
-.1
-.05
0
.3
.2
.1
.05
0

$\frac{Z}{Z_i}$

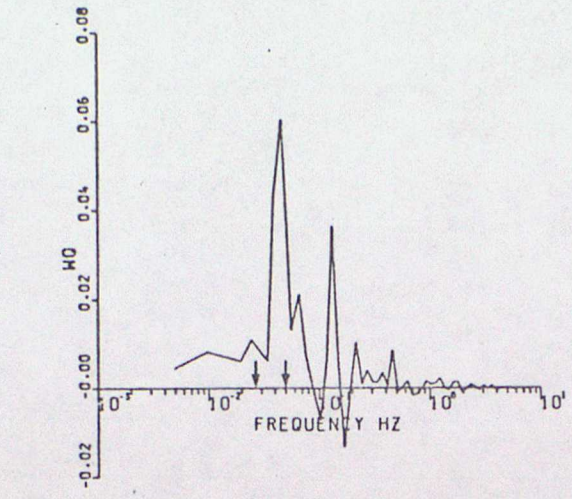

0.86

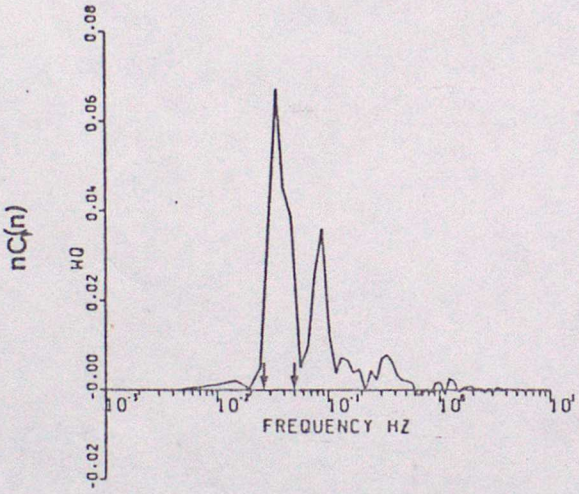

0.67

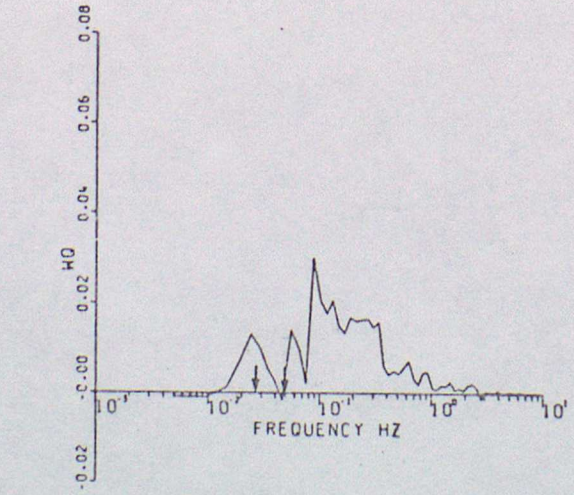

0.28